Chemical Engineering Journal 490 (2024) 151800

Contents lists available at ScienceDirect

Chemical Engineering Journal

journal homepage: www.elsevier.com/locate/cej

A high performance triboelectric nanogenerator using assembled sugar naphthalimides for self-powered electronics and sensors

Arun Kumar Rachamalla [a], Madathil Navaneeth [b], Tohira Banoo [a], Deepshikha [a], Vara Prasad Rebaka [a], Yogendra Kumar [a], Rakesh Kumar Rajaboina [b,*], Subbiah Nagarajan [a,*]

[a] Assembled Organic and Hybrid Material Lab, Department of Chemistry, National Institute of Technology Warangal, Hanumakonda 506004, Telangana, India
[b] Energy Materials and Devices Lab, Department of Physics, National Institute of Technology Warangal, Hanumakonda 506004, Telangana, India

ARTICLE INFO

Keywords:
Molecular assembly
Gels
Naphthalimides
Triboelectric nanogenerator
Self-powered electronics

ABSTRACT

A new class of N-glycosyl naphthalimide ricinoleate (NGNR) amphiphiles were generated using environmentally friendly reaction conditions in good yields. To investigate the potential applications of NGNR amphiphiles within the realm of supramolecular materials, molecular self-assembly experiments were conducted extensively across a diverse range of solvents and oils and observed the gel formation. Molecular-level interactions and assembly patterns were investigated by employing FTIR, SAXRD, UV–vis, and fluorescence spectroscopy, and a plausible assembly mechanism was proposed. The morphology of the supramolecular architecture was identified by scanning electron microscopy. Additionally, rheological studies provided insight into these soft materials' strength and processability. Further, in the process of fabricating a triboelectric nanogenerator (TENG) device, silicone rubber serves as an electron acceptor and assembled NGNR serves as an electron donor. The developed TENG demonstrated a significant improvement in performance over TENG made with amorphous NGNR, with output voltage, current, and power density of 410 V, 100 μA, and 5.1 W/m^2, respectively, highlighting the importance of the assembly process. Furthermore, TENG is used to continuously power up small electronic device (calculator), which is useful in building self-powered electronic devices. Lastly, due to its high sensitivity and stability, the TENG was used to detect the humidity of the environment in the food processing, textile, and agriculture sectors. The change in TENG response is notably significant up to 70 % relative humidity (RH). This work showcases the development of self-powered humidity sensors.

1. Introduction

The era of the Internet of Things (IoTs) is uprising with the overall development of artificial intelligence technology [1,2], fifth-generation networks [1,2], portable electronics [3,4], and sensor networks [5,6], which require abundant energy and greater precession. To fulfill the requirements of IoTs, universally sustainable, reliable, and abundant power supplies are necessitated, wherein Triboelectric nanogenerators (TENG) display several merits, including low-cost manufacturing, a broad selection of materials, high energy conversion efficiency at low motion frequencies, strong scalability, lack of pollution, and with lightweight fabrication [7–10]. It has the ability to generate electricity by harvesting random mechanical energy from the surroundings based on contact electrification and electrostatic induction phenomena [11,12]. Basically, contact electrification, or triboelectrification, is a physical phenomenon that explains the transfer of electrons between two materials when they come into physical contact, which is based on the electron affinities of the materials used. In particular, materials with higher electron affinity act as electron acceptors, whereas other materials act as electron donors. However, in the fabrication of TENG,

Abbreviations: IoTs, Internet of Things; TENG, Triboelectric nanogenerators; NGNR, N-glycosyl naphthalimide ricinoleate; GCNA, Gluconolactone conjugated naphthalimide amphiphiles; GRAS, Generally Recognized as Safe; FDA, Food and Drug Administration; WHO, World Health Organization; FAO, Food and Agriculture Organization; NMR, Nuclear Magnetic Resonance; FT-IR, Fourier-transform infrared spectroscopy; DMSO, Dimethyl sulfoxide; CGC, Critical gelation concentration; Tg, Sol-to-gel transition temperature; HLB, Hydrophilic Lipophilic Balance; ATR-FTIR, Attenuated Total Reflectance Fourier Transform Infrared Spectroscopy; XRD, X-Ray diffraction; UV, Ultraviolet; AIE, Aggregation Induced Emission; SEM, Scanning electron microscopy; LVE, Linear viscoelastic region; PMMA, Polymethyl methacrylate; FEP, Fluorinated ethylene propylene; AC, Alternating Current; DC, Direct current; RH, Relative humidity.

* Corresponding authors.
E-mail addresses: rakeshr@nitw.ac.in (R. Kumar Rajaboina), snagarajan@nitw.ac.in (S. Nagarajan).

https://doi.org/10.1016/j.cej.2024.151800
Received 12 March 2024; Received in revised form 18 April 2024; Accepted 28 April 2024
Available online 4 May 2024

materials selection plays a vital role in expanding the scope of green energy harvesting technologies and gaining maximum output performance with mechanical stability upon repetitive contact [13–15]. In 2012, Wang and co-workers developed the first TENG [16]; later, various groups utilized synthetic, natural polymers, and inorganic materials, including MOFs, metal oxides, and metals. The comparison of different materials based on TENG and their output performance is shown in Table S1.

Even though TENG was used for various applications [17], its utility in the fabrication of self-powered sensors is in huge demand. In the recent past, various materials [18–23] were used for the fabrication of sensors for environmental and safety monitoring, wearable electronics, and diagnostic devices [24–30]. However, the use of assembled small molecules in the fabrication of sensor devices using TENG is limited. It is worth mentioning that great progress has been made in selecting materials for the fabrication of TENG, and the potential use of assembled organic materials has been explored the least. Recently, our research group first reported the use of self-assembled supramolecular gel derived from naphthalimide-based amphiphiles in the fabrication of TENG [31]. Later, Mallik and co-workers derived π-electron-rich amino acids based amphiphiles and demonstrated them as a promising power source [32]. In assembled organic systems, molecular design and the resultant electron density generated by the bottom-up assembly process play a significant role.

In general, nature utilizes carbohydrates, proteins, and fats, which are widely abundant, for the generation of required energy [33–35]. Supramolecular assembly of these classes of molecules generates nano energy in nerves and muscles, which are crucial for movement, memory, and many other physiological processes [36,37]. However, among these, carbohydrates are an interesting class of molecules having several chiral centers existing in living organisms, such as glycolipids, glycoproteins, proteoglycans, etc., and perform various brilliant tasks [38–41]. Specifically, the functions of such systems are related to architecture, energy metabolism, and molecular interactions [42–45]. For the fabrication of next-generation molecular materials, carbohydrates play an indispensable role as building blocks because of their biocompatibility, natural abundance, and biodegradability [46,47]. By considering the salient features of carbohydrates, in this work, we have used carbohydrates, in particular monosaccharides, to synthesize N-glycosyl naphthalimide ricinoleate amphiphiles (NGNRs). The selection of naphthalimide as an aglycon part is because of its immense applications in molecular materials. 1,8-Naphthalimides have been widely used in materials and medicine because of their excellent structural stability, extended conjugation, high fluorescence quantum yield, photo-stability, and large stroke shift [48–53]. Utilizing these assembled organic materials in the fabrication of TENG opens up new avenues for energy harvesting technology. Recently, in one of our reports, we have demonstrated the use of self-assembled gluconolactone conjugated naphthalimide amphiphiles (GCNA) as an electron donor layer in combination with the PDMS as an electron acceptor in TENG, which generated an output voltage, current, and power density of ~ 250 V, 40 μA, and ~ 622 mW/m^2 respectively [31].

For constructing bottom-up assembled energy materials, molecules displaying a precise combination of hydrophobic and hydrophilic units are essential. Based on our expertise in molecular assembly, we have carefully designed the synthesis of NGNR by choosing monosaccharides as the hydrophilic part, naphthalimide core as π-π stacking unit, and ricinoleic acid, generally referred to as 12-hydroxy-9-*cis*-octadecenoic acid obtained from castor oil, as a hydrophobic part. Monosaccharides and Ricinoleic acid are Generally Recognized as Safe (GRAS) by the Food and Drug Administration (FDA). In particular, the World Health Organization (WHO) and the expert committee of the Joint Food and Agriculture Organization (FAO) have approved a daily intake of castor oil, a precursor of ricinoleic acid, up to 0.7 mg/kg body weight [54]. Consequently, NGNR used for the fabrication of TENG is derived from environmentally friendly resources using a simple synthetic strategy. A TENG was constructed by a bottom-up assembly process using the molecular gelation concept through a more sustainable pathway that would open a gateway to green energy harvesting. The modification in hydrophilic and hydrophobic part rendered a significant enhancement in output voltage, current, and power density of 410 V, 100 μA, and 5100 mW/m^2, respectively. The influence of molecular structure in the fabrication of assembled organic energy materials has not reported to date and our research group is exclusively working on the fabrication of assembled organic nano energy harvesting devices.

In this paper, we have synthesized a series of NGNR using a sustainable protocol in good yields, whereas the literature reported methods involve multi-step synthesis, use of highly complex protection and deprotection strategies, limited substrate scope, involves column chromatography purification, and ended up with poor yields. Molecular self-assembly studies of synthesized NGNRs in various solvents using non-covalent interactions such as hydrophobic interactions, hydrogen bonding, π-π interactions, and van der Waals forces generated a 3D-fibrillar network, wherein the solvent is trapped and formed a gel. Most importantly, from the application point of view, the bottom-up assembly mechanism of NGNR is proposed based on the FT-IR, SAXRD, UV–vis, and fluorescence techniques. Inspired by nature's energy harvesting using the molecular assembly phenomenon, we have demonstrated a novel energy harvesting and utilization strategy. In general, the naphthalimide core is reported as an electron acceptor [52]. In contrast, in the present report, molecular assembly significantly enhanced the electron density in the naphthalimide and turned into an electron donor, as evidenced by our studies. This work offers new insight into the fabrication of organic TENG based on the bottom-up assembly process and shows promising potential for self-powered electronics and a humidity sensor application.

2. Results and discussion

Initial optimization of reaction conditions: Naphthalimides are one of the most versatile cores displaying unique optoelectronic properties [52]. Modifying naphthalimides by integrating varieties of structural units and functional groups was significant among the researchers [55,56]. Recently, our group has optimized the reaction condition suitable for the synthesis of N-glycosyl naphthalimides using batch process using conventional methods. However, the research of alternative, simple, and environmentally friendly approaches for the synthesis of chemicals of industrial significance is essential. In this report, a continuous flow reactions have been performed to obtain 3-amino-N-(ricinoleic acid hydrazide)-1,8-naphthalimides (**3**), from 3-nitro-1,8-naphthalic anhydride (**1**) with methyl ricinoleate hydrazides (**2**), which includes condensation followed by in situ reduction using Fe in AcOH. In organic synthesis, control of temperature and pressure is a critical factor in achieving the requisite activation energy, leading to the effective desired product formation. In order to overcome the limitations faced in the conventional batch process, we have adopted a flow chemistry method by integrating the condensation and reduction processes. By harnessing the high temperature and high-pressure flow reactions in the heterogeneous phase using Fe catalyst, we were able to generate the desired compound **3** in good yields. Fig. S1 represents the response of the product with respect to the temperature and time. Initially, the reaction was carried out at 80 °C, 2 bar pressure with a flow rate of 100 μL, and observed a 60 % conversion. With this interesting result on hand, we were curious to optimize a continuous generation of compound **3** in high yield using a high temperature and high-pressure flow reactor. For high-temperature and high-pressure applications, the stainless-steel coil reactor is the obvious material of choice.

By fixing the flow rate of substrates at 100 μL/min, 2 bar pressure, we have tuned the temperature and investigated the % of conversion into a product. The subsequent increase in the temperature of the flow reactor from 80 °C to 300 °C with an increment of 20 °C generated a steady rate of increase in the reaction with a maximum conversion rate of 94 %. By increasing the retention time of the reactants in the steel coil flow

reactor by reducing the flow rate up to 100 μL/min at 200 °C, 2 bar pressure generated a continuous production of compound **3** with traces of polar impurities, which were purified using recrystallization in EtOH. It is worth mentioning that in the condensation reaction using a flow reactor, the unsaturation present in the ricinoleate moiety did not interfere, and further reduction of the nitro group was also facilitated smoothly (Fig. 1).

3-amino-N-(ricinoleic acid hydrazide)-1,8-naphthalimides **3** with various monosaccharides 4 using $(NH_4)_2SO_4$ as a catalyst in methanol was performed in a batch reactor at a higher temperature. Reactions performed at 80 °C furnished the desired product after the prolonged reaction time of 24 h in moderate yields (Fig. 1). Further, an increase in temperature up to 120 °C rendered the desired product in excellent yield within 4 h. It is worth stating that a further increase in temperature results in a decrease in the yield of the desired amphiphile 5, which is attributed to the Amadori rearrangement. This type of non-enzymatic Amadori rearrangement occurs at high temperatures due to sugar caramelization, which is an undesired and uncontrolled event. Overall, the key features of our optimized condition involve no protection and deprotection of sugars, formation of exclusively β-anomeric product, no formation of undesired products in the entire reaction sequence, and the only side products obtained is one molecule of oxygen and two molecules of water with an excellent yield of desired product without any complicated workup and column chromatographic purification (Fig. 1).

All the synthesized NGNRs were well characterized using NMR, FT-IR, and mass spectral techniques. Generally, the anomeric proton of a sugar moiety displays a coupling constant of $J \leq 4$ Hz for α-anomer, and $J > 4$ Hz for β-anomer. The calculated coupling constant $J = 5.2$ Hz for the anomeric proton of NGNR **5a** resonating at 4.21 ppm as a doublet in the deuterium exchange ^{1}H NMR spectrum confirms the formation of β-anomeric product.

Self-assembly of carbohydrates is an important process generally observed in all living organisms, which can produce a variety of

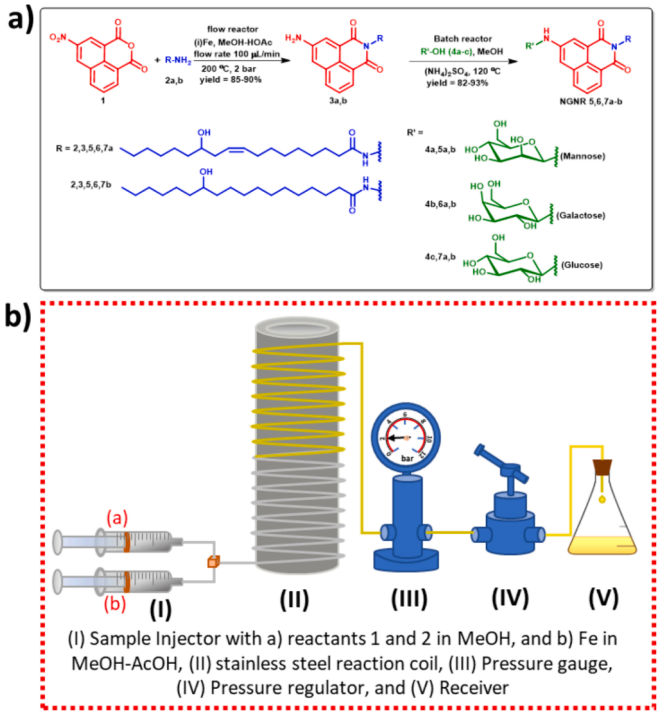

Fig. 1. (a) Synthesis of N-glycosyl-3-amino-N-(ricinoleic acid hydrazide)-1,8-naphthalimides (NGNRs) from 3-nitro-1,8-naphthalic anhydride and methyl ricinoleate hydrazides. (b) Pictorial representation of optimized flow reactor. The reproducibility of the optimized chemical process is checked with various substrates and gram scales.

nanostructures with unique properties and have a key role in biological signal transmission, cell recognition, and cell–cell communication. The gelation abilities of synthesized NGNR compounds were studied in a wide variety of solvents and oils (Table S2).

The formation of the gel was identified using "the stable to inversion of container" method at room temperature. Gelation studies revealed that the synthesized NGNRs could able to form organogel in xylenes and hybrid hydrogel in DMSO-H_2O in the ratio of 4:6 (v/v). Organogel formed in xylenes displayed good strength, whereas the hybrid hydrogels were soft with the CGC 6 %; even a little shaking could break the gel. We were very curious to investigate the gelation capability of NGNRs in o-xylene, m-xylene, and p-xylene. At this juncture, the organogel formed by NGNRs in m-xylene is stronger than the gel formed in o-xylene and p-xylene, which is ascribed by gel-to-sol transition temperature. All six NGNRs **5,6,7(a&b)** furnished an opaque yellow gel in m-xylene on cooling to room temperature and were stable at room temperature for more than three months. The critical gelation concentration (CGC) of NGNR **5a**, **6a**, and **7a** in m-xylene is 1.5 %, and **5b**, **6b**, and **7b** is 1 % (wt/v), respectively. The representative images of the gel formed by NGNR **5b**, **6b**, and **7b** are given in Fig. 2**a**. Interestingly, NGNR **5b-7b** without unsaturation in the hydrophobic unit displayed better gelation ability of 1 % wt/v, whereas the compounds **5a-7a** having unsaturation in the hydrophobic unit formed a relatively higher CGC of 1.5 % wt/v.

Further, we have examined the thermo-reversible nature of the organogel through repeated heating and cooling cycles. Remarkably, even after 25 cycles, these gels remained stable because of the reversible intermolecular interactions. To ascertain the strength of the gel, we meticulously identified the sol-to-gel transition temperature, T_g, for organogel formed by NGNR **5,6,7(a &b)**. The designed amphiphiles possess ricinoleate unit as a hydrophobic tail, naphthalimide as a π-π stacking component, and monosaccharides as hydrophilic head groups, respectively. It is observed that the organogel formed from **5b**, having mannose as a hydrophilic unit, displayed a higher $T_g = 102$ °C, when compared to its epimer **7b**, derived from glucose (87 °C). In addition, NGNR **6b**, derived from galactose, exhibited $T_g = 91$ °C, which is also an epimer of compound **7b**. These interesting results strongly indicate that the process of epimerization has the potential to significantly modify the gel strength through intermolecular interactions, which directly reflects on supramolecular architecture. Investigation on gelation ability and T_g revealed that **5b**, **6b**, and **7b**, possessing a similar Hydrophilic Lipophilic Balance (HLB) level, create a gel with the same CGC. However, the strength of the gel differs due to the orientation of the –OH groups within the 3D lattice, affecting the intermolecular H-bonding. Measurements of the concentration-dependent T_g exhibited a gradual rise and reached a plateau once the NGNRs solution reached the saturation point (Fig. S2, S3). Among the various NGNRs synthesized, **5b** with higher Tg = 102 °C and CGC of 1 % (wt/v) has been considered as a model substrate for further investigation and represented as NGNR **5b**.

To understand the self-assembly mechanism, molecular-level insights are necessitated. Various intermolecular interactions such as hydrogen bonding, π-π stacking, anionic –π and cationic –π and van der Waals displayed by a molecule play a crucial role in the assembly mechanism. Hydrogen bonding is ubiquitous in nature and plays a vital role in the structure and function of various supramolecular architecture including the assemblies of DNA and RNA helices. Fourier transform infrared spectroscopy is the best tool to study the intermolecular interactions with respect to the functional groups. We have recorded the Attenuated Total Reflectance Fourier Transform Infrared Spectroscopy (ATR-FTIR) spectrum for the needle-like crystalline NGNR **5b** and its xerogel (Fig. 2**b**). NGNR **5b** in crystalline state displayed peaks for –OH and –NH stretching at 3350 cm^{-1} and 3234 cm^{-1} respectively. During the process of gelation, owing to the entrapment of solvent and flexible fibrillar aggregation, both –OH and –NH stretching frequencies displayed a shift towards a higher wavenumber region and were observed at 3458 cm^{-1}. In the crystalline state, stretching frequencies of carbonyl group, amide 1, amide 2, –C = C-, and bending frequencies of C-H

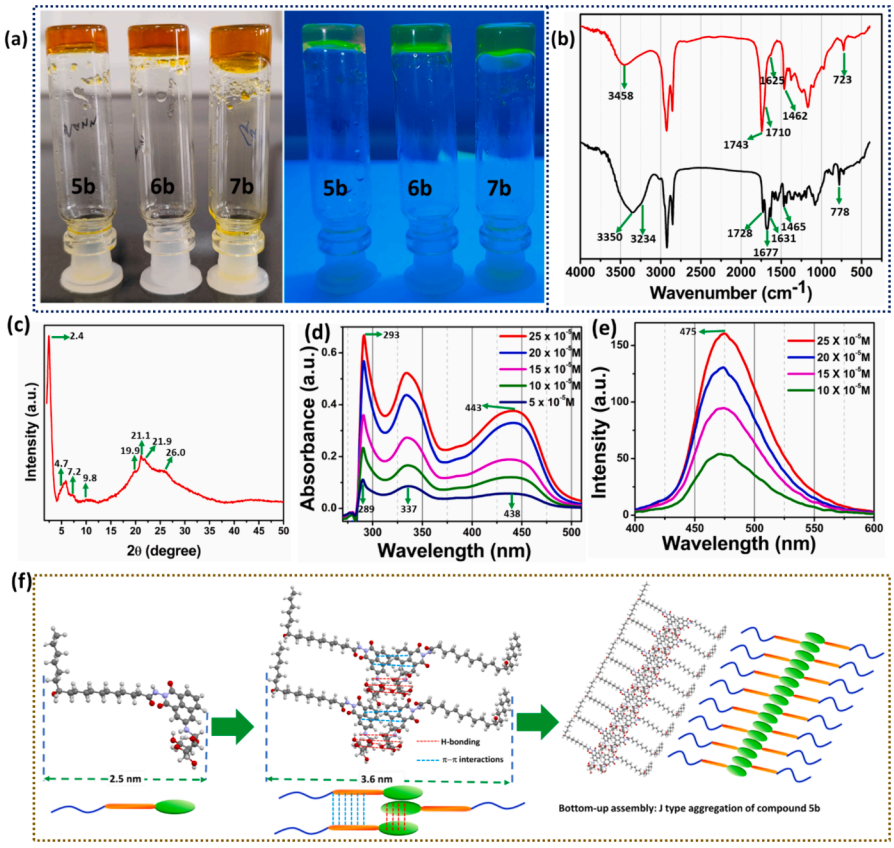

Fig. 2. (a) Images of the gel formed by NGNR **5b-7b** in m-xylene under normal and UV light (CGC = 1 % wt/v). (b) A comparison of FT-IR spectra of NGNR **5b** in xerogel state (red), and amorphous state (black). (c) The XRD pattern of a xerogel was obtained from NGNR **5b**. (d) UV–vis, and (e) fluorescence titration of NGNR **5b** dissolved in gelling solvent xylene [λ_{ex} = 289 nm]. (f) A schematic representation of bottom-up assembly of NGNR **5b** to generate *J*-type aggregated intertwined lamellar sheet structure.

appeared at 1728, 1677, 1465, 1631, and 778 cm^{-1}, whereas in the xerogel state, all these peaks displayed appreciable shift and observed at 1743, 1710, 1462, 1625 and 723 cm^{-1} respectively. FTIR analysis clearly reveals the involvement of various groups in molecular self-assembly via intermolecular interactions. It is worth mentioning that the peak corresponds to the stretching frequency of aromatic −C = C- appeared at 1631 cm^{-1} in the crystalline state displayed a shift to lower wavenumber region revealed the involvement of aromatic moiety of naphthalimide in π-π stacking. FTIR analysis disclosed that the molecular arrangement in the crystalline state is different from the xerogel state.

Predicting the molecular arrangement within the supramolecular gel is exceptionally challenging, as the structure and characteristics depend on the geometry and arrangement of building blocks in a three-dimensional lattice. Nonetheless, by understanding the intermolecular interactions among gelators from FTIR analysis, we can predict the packing through the small angle-XRD (SAXRD) technique. The xerogel obtained from NGNR **5b** displayed 2θ = 2.4°, 4.7°, 7.2°, 9.8° corresponding to the interplanar spacing (d-spacing) at 3.6, 1.8, 1.2 and 0.9 nm, respectively. XRD peak analysis revealed the Bragg's reflection following a consistent pattern of 1, ½, 1/3 and 1/4 (Fig. 2**c**). Peaks displayed at 19.9°, 21.1°, 21.9°, and 26.0° corresponds to the π-π stacking arrangement. Intermolecular interactions facilitate the molecular self-assembly, creating a 3-D fibrillar network architecture measuring a length of 3.6 nm as determined by XRD, which is higher than the end-to-end molecular length of NGNR. The end-to-end molecular length of NGNR **5b** is 2.5 nm, calculated from the energy-minimized structure of NGNR **5b**. This result suggests the presence of a double layer stabilized by intermolecular H-bonding.

UV absorption and fluorescence characteristics are integral in the design and functionality of a broad spectrum of electronic devices; these properties enable fine-tuned color control, data transmission, energy conversion, and substance identification. A detailed investigation on absorption and emission characteristics of a conjugated molecule opens a pathway to establish the efficiency and performance of electronic devices. Absorption spectra of NGNR **5b** in gelling solvent, m-xylene is given in Fig. 2**d**. In the UV–visible spectra, three distinct and well resolved peaks centered at 289, 337 and 438 nm are observed, and these bands can be ascribed to the π–π* transition of the amide group, n–π* transition of the naphthalimide, respectively. Notably, as the concentration of the gelator increases, the peak centered at 289 and 438 nm displayed a redshift to 293 and 443 nm respectively. The red shift displayed by NGNR **5b** upon increase in concentration clearly indicates the emergence of *J*-type aggregation results in supramolecular organization.

Aggregation Induced emission (AIE) is a distinctive photophysical phenomenon exhibited by specific conjugated organic molecules. Unlike the conventional behavior of fluorophores, which becomes less emissive upon aggregation, AIE molecules exhibit increased enhanced emission when they aggregate into an assembled state. Assembled materials displaying AIE are instrumental in a wide array of applications, including printed circuit boards, electronic gadgets, security, bio and chemical sensors, energy harvesting, and electronic communication systems. Fig. 2**e** represents the emission behavior of NGNR **5b** in gelling solvent m-xylene at various dilutions. Upon increasing the concentration, a gradual increase in the emission intensity suggests the existence of AIE. Based on the FTIR, SAXRD, and UV absorption studies, we have proposed the molecular self-assembly mechanism, which is given in Fig. 2**f**.

After understanding the assembly mechanism of NGNR 5b and its photophysical behavior, we examined the gels' morphology using scanning electron microscopy (SEM), as shown in Fig. 3**a-c**. The gel

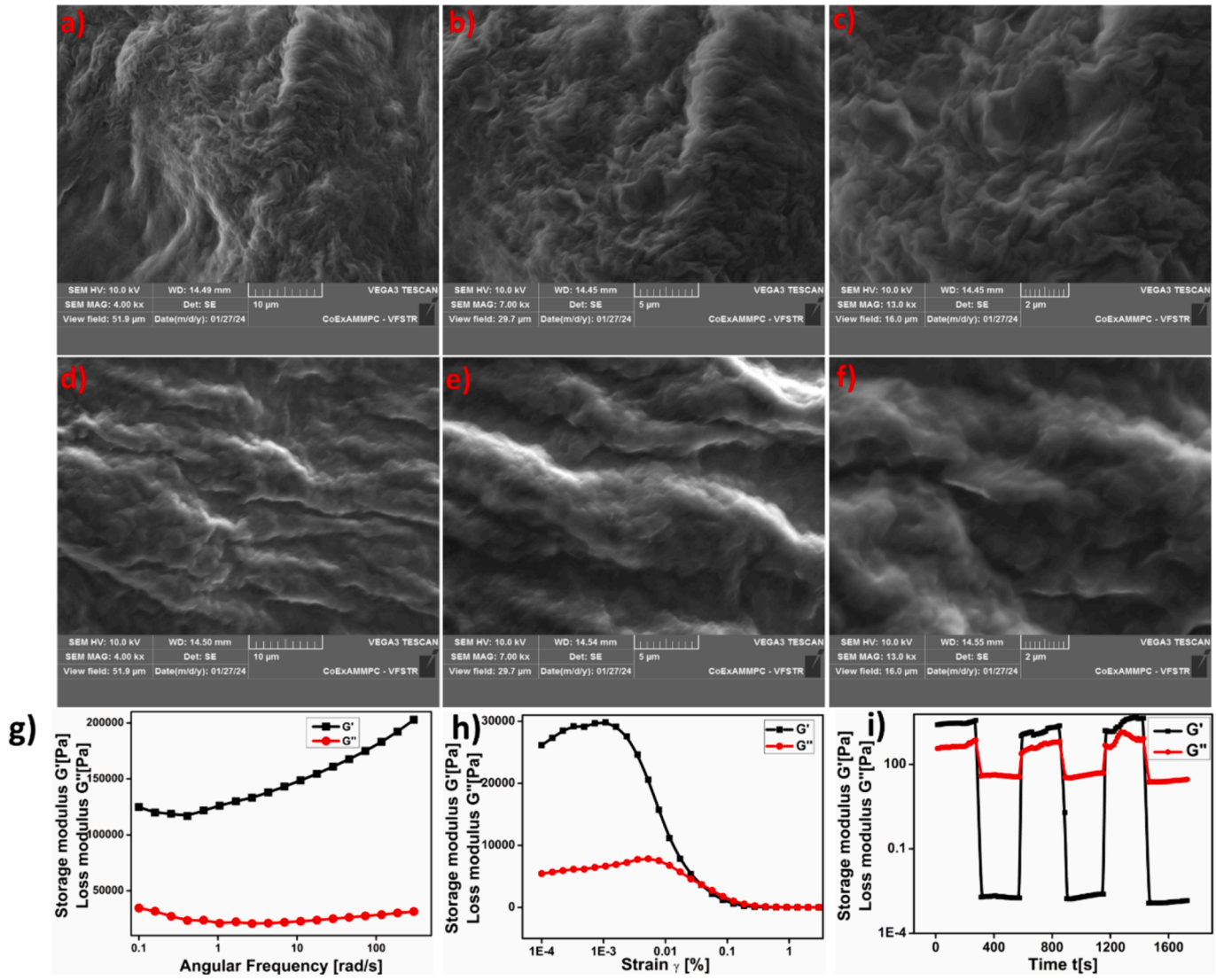

Fig. 3. SEM images of the xerogel formed by NGNR **5b** in various magnifications (a, 10 μm; b, 5μm; c, 2μm), and **6b** (d, 10 μm; e, 5μm; f, 2μm) in m-xylene. (g) angular frequency, and (h) strain amplitude dependency of G' and G" of the gel formed by NGNR **5b** in m-xylene. (i) Thixotropic behavior investigation using continuous strain ramp-up and ramp-down measurements of the gel formed by NGNR **5b** in m-xylene.

formed by NGNR **5b** in xylene displayed intertwined lamellar sheet-like morphology obtained by intermolecular interactions. It is worth mentioning that SEM analysis of another NGNR, **6b** in xylene, generated an intertwined globules sheet (Fig. 3**d-f**). Morphological analysis clearly revealed that even changes in the orientation of sugar hydroxyl groups can drastically affect the morphology, reflecting on the material performance. As per the literature, surface morphology plays a crucial role in TENG fabrication [57–59], since the device efficiency, reliability, and versatility depend on how the surface characteristics are designed and engineered. This surface characteristics of materials enable TENGs to be adapted for various energy harvesting applications [60–62]. It is worth mentioning that NGNR **5b** displayed better performance than **6b**, as indicated by preliminary TENG studies.

The key consideration when utilizing gel materials to fabricate TENGs is their ability to be flexible, mechanical strength, and versatile enough to satisfy the demands of TENGs as flexible wearable electronics. The Mechanical strength is an important parameter of the materials used in TENG fabrication because it should not undergo deformations while processing, such as stress or stain, frequency, or temperature. Rheology is the best tool to measure the processability of gels and can provide important information on the strength and thermoreversibility. The frequency sweep experiment of gel formed by NGNR **5b** in m-xylene furnished a greater value of storage modulus G' compared to the loss modulus G" throughout the range of analysis disclosed its strength (Fig. 3**g**).

Stress or strain sweep experiment was conducted by varying the amplitude of input signal at constant temperature and frequency, a slight fold or deformation in supramolecular structure is observed beyond the critical strain (γ_c) value of 0.002 %, and complete gel to sol transition was observed at $\gamma = 0.038$ %, the greater value of G' compared to the G" within the linear viscoelastic region (LVE) suggest a good mechanical strength of the gel (Fig. 3**h**). Thixotropic nature of the gel formed by NGNR **5b** was investigated by a continuous step-strain experiment (Fig. 3**i**). On applying a constant strain (100 %), G' is found to be lower than the G", indicating the deformation of 3D supramolecular network in organogel. Upon reducing the strain to 1 %, the greater value of G' compared to the G", revealed the rapid recovery nature of the gel to its original form by reconstructing the supramolecular network. Thixotropic nature of the gel was consistent even after three cycles, which clearly supports the good strength and processability of the gel for the use as a triboelectric layer in the fabrication of TENG. It is worth mentioning that the gel displayed thixotropic behavior on

simple shaking and resting. The hypothesis for the thixotropic behavior of the gel is the gelator makes the stronger hydrogen bonding interaction between the sugar molecules, establishing the one-dimensional aggregate, and weak van der Waals interactions between the long aliphatic chain form the three-dimensional architecture. The shear strain produced breaks only the weak van der Waal interaction but not the hydrogen bonding, which results in gel deformation. Upon releasing the shear strain, three-dimensional networks regenerate through the recovery of intermolecular interactions, thereby gel gets regenerated.

TENG device fabrication: Fig. 4**a** shows the schematic of the TENG and its components. The TENG device was fabricated using NGNR **5b** film and silicone rubber deposited on aluminium as triboelectric layers and aluminium as electrodes for TENG. These two triboelectric layers were attached to two cardboards sheets on top of each other and separated with sponge spacers to operate TENG in vertical contact separation mode (VCS), as shown in Fig. S4. Finally, both electrodes were connected with electrical wires, and the electrical outputs of the TENG were measured using a digital oscilloscope (GW-instek, GDS −1102B) and low noise current preamplifier (SRS, SR 570). Further, additional TENG devices were fabricated for fixed NGNR **5b** film and variable opposite frictional layers such as aluminium, polymethyl methacrylate (PMMA), and fluorinated ethylene propylene (FEP). The stability of the TENG device was performed using an in-house developed tapping machine. It is worth mentioning that the TENG developed with amorphous NGNR **5b** displayed low output because of the absence of molecular assembly.

The electrical characteristics of TENG devices, utilizing a fixed NGNR **5b** film against various opposing triboelectric layers, are depicted in Fig. 4**b**. Among these configurations, the highest performance was achieved with a device comprising a NGNR **5b** film on an aluminium substrate paired with silicone rubber, achieving an open-circuit voltage of 410 V and a short-circuit current of 100 μA. This specific pairing was selected for additional measurements of the device. The differential response of the TENG devices can be attributed to the electron-accepting and donating properties of the materials involved in frictional contact. The NGNR **5b** film acts as an electron donor due to its chemical bonding and surface characteristics. Consequently, the output is relatively low when the NGNR film is combined with another electron-donating material, such as aluminium. However, pairing the NGNR **5b** film with an electron-accepting material, like silicone, significantly enhances the device's output. This behavior underscores the electron-donating attribute of the NGNR **5b** film.

Further, a switching polarity test of the TENG device was performed, and the results are presented in Fig. 4**c-d**. This confirms that the voltage and current output are generated from TENG alone, not any noise signal from the instrument. Fig. 4**e** presents the variation of voltage and current output of the TENG at different load resistances. The voltage increases with load resistance and reaches saturation level after 10 MΩ, while the current decreases with load resistance and gets saturated after 10 MΩ. The observed load characteristics of TENG are similar to the existing reports [63–65]. The instantaneous power density of the TENG was calculated using the P = V*I/A formula, and the results are presented in Fig. 4**f**. The TENG reaches a maximum power density of 5.1 W/m^2 at a load resistance of 10 MΩ, from the maximum power transmission theorem, which can be considered as an impedance matching condition [66].

Moreover, the TENG device underwent a stability and durability test involving a consistent tapping force applied by a machine for 10,000 cycles, demonstrating remarkable stability (SI, Video V1). Following this, the device was subjected to manual tapping for an additional 600 cycles, with the outcomes showcased in Fig. 4**g**. Impressively, the TENG device maintained its initial output level even after 10,600 total cycles, underscoring its durability. Furthermore, images of the NGNR **5b** film, both prior to and following the 10,000-cycle test, are displayed in Fig. S4. These visuals confirm the NGNR **5b** film's mechanical resilience and strong adhesion to the aluminium substrate, with no evidence of cracking observed on its surface. Further, we used a bridge rectifier circuit to convert the AC signal produced by the TENG into a DC signal, as shown in Fig. 4**h**. A 100 μF capacitor was charged to 1.25 V in 280 sec

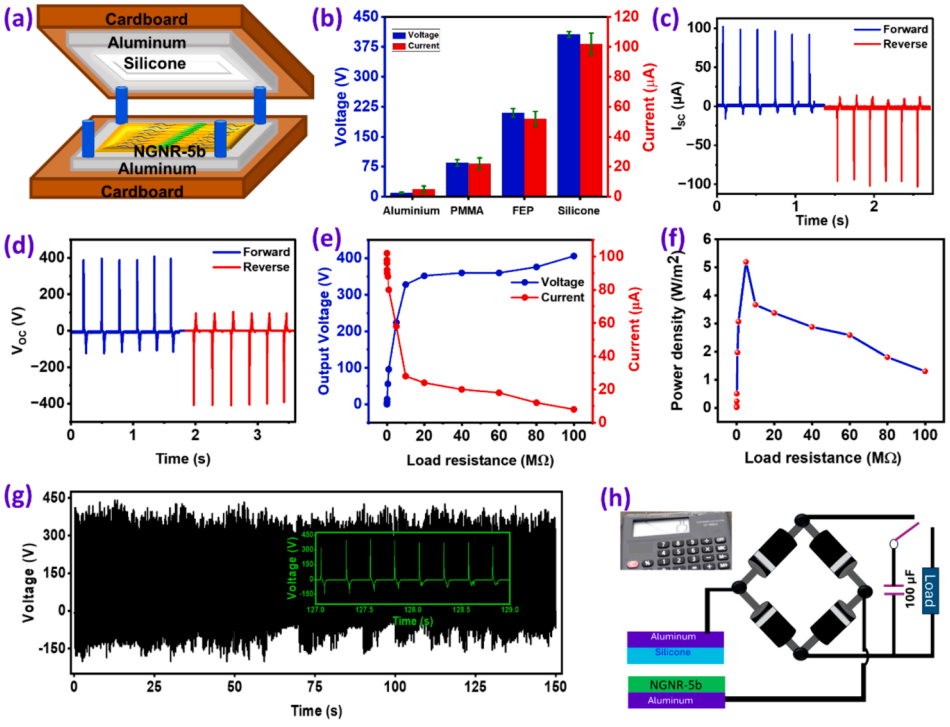

Fig. 4. (a) Schematic of the TENG device, (b) TENG response with different frictional layers with statistical analysis; (c-e) switching polarity results of (c) Voc, (d) Isc, (e) load resistance versus output voltage and current, (f) the instantaneous power density as a function of load resistance, (g) stability of TENG electrical response for 600 cycles of hand tapping, (h) photograph of the digital calculator continuously powered with TENG. Experiments are performed in triplicate under optimized conditions to check the reproducibility and repeatability.

using a linear motor. Later charged voltage was utilized for the continuous operation of the calculator (Fig. 4**h**), and the capacitor was simultaneously charged by TENG (SI, Video V2). This demonstration shows the potential of TENG in building self-powered systems.

TENGs have a wide range of applications due to their ability to convert low-frequency mechanical energy into electricity. Further, TENGs output is very sensitive to the surface condition of the frictional layers, making them suitable for applications in sensing chemicals, gases, and humidity [67–69]. TENG can be used as a sensor to make them low-maintenance and cost-effective [70]. The present report explores TENG in humidity sensing applications using an in-house developed sensing setup, as depicted in Fig. 5**a**. During the experiments, the TENG device was manually tapped while introducing water vapor from a humidifier into the testing chamber in a controlled manner (SI, Video V3). The electrical output of the TENG was measured across different relative humidity levels ~ 47 %, 58 %, 69 %, 78 %, 88 %, and 95 % and the findings are presented in Fig. 5**b**. The results clearly indicate a gradual decrease in the voltage output from 142 to 11 V as the humidity level increases (Fig. 5**c**), illustrating a linear correlation between the output voltage and varying levels of humidity.

This linear relationship underpins the potential of TENGs as self-powered humidity sensors. Fig. 5**d** shows the photographs of the LEDs powered by TENG under different humidity conditions, and it clearly indicates the decrement in the output voltage with humidity (SI, Video V4). Typically, the performance of a humidity sensor is characterized by the electrical response (such as resistance, voltage, or current) of the device, as given by the formula [71,72].

$$\text{Response} = \frac{(V_0 - V_{RH})}{V_0} \times 100\% \quad (1)$$

where V_0 is TENG output at low RH value (47 %) when external no water vapor is introduced into the test chamber and V_{RH} is TENG output under different humidity conditions. The TENG humidity sensing response is presented in Fig. 5**e**.

The effect of humidity on the TENG response is well reported in the literature [73]. In most cases, the decrease in the TENG output is attributed to the neutralization of surface charges on the triboelectric layers by adsorbed water molecules and same can be applied for the present study. [67,71,74–77]. Additionally, the presence of hydrophilic functional groups on the surface of the triboelectric layers tends to increase water adsorption, thereby improving the device's sensitivity to humidity. It has been observed that the change in TENG response is notably significant up to 70 % relative humidity (RH) and becomes less pronounced beyond this point. This pattern can be explained by the increased number of water molecules adsorbed on the triboelectric layers fabricated by using assembled NGNR **5b**. At higher humidity levels, the assembled NGNR 5b experience a decreased electron density because of in situ tuning of pattern, followed by the reduction in electrostatic charges generated during contact electrification (Fig. 5**f**).

3. Conclusion

We have developed a continuous flow method for the generation of N-glycosyl naphthalimide ricinoleate (NGNR) amphiphiles in good yield using an environmentally friendly chemical process. Inspired by nature's energy harvesting using molecular assembly phenomenon, we have demonstrated a new strategy for energy harvesting and utilization. An important aspect of the demonstrated system is the up-conversion of electron-deficient naphthalimides into electron-rich species by molecular assembly. Using the fabricated nanogenerator, a large potential can be generated and used for operating self-powered electronic devices. In addition, the device fabricated from assembled organic material is low-cost, stable, reliable, and easy to fabricate, making it potentially advantageous for practical applications. The self-powering nature avoids the use of an external power supply, and its highly sensitive molecular architecture facilitates the detection of relative humidity in the food processing, textile, and agriculture sectors.

CRediT authorship contribution statement

Arun Kumar Rachamalla: Methodology, Investigation, Analysis, Writing – original draft. **Madathil Navaneeth:** Investigation on TENG. **Tohira Banoo:** Methodology, Data acquisition help. **Deepshikha:** Synthesis and Data acquisition help. **Vara Prasad Rebaka:** Methodology, Data acquisition help. **Yogendra Kumar:** Methodology, Data acquisition help. **Rakesh Kumar Rajaboina:** Investigation of TENG, Methodology of TENG, Writing – review & editing, Software, Formal

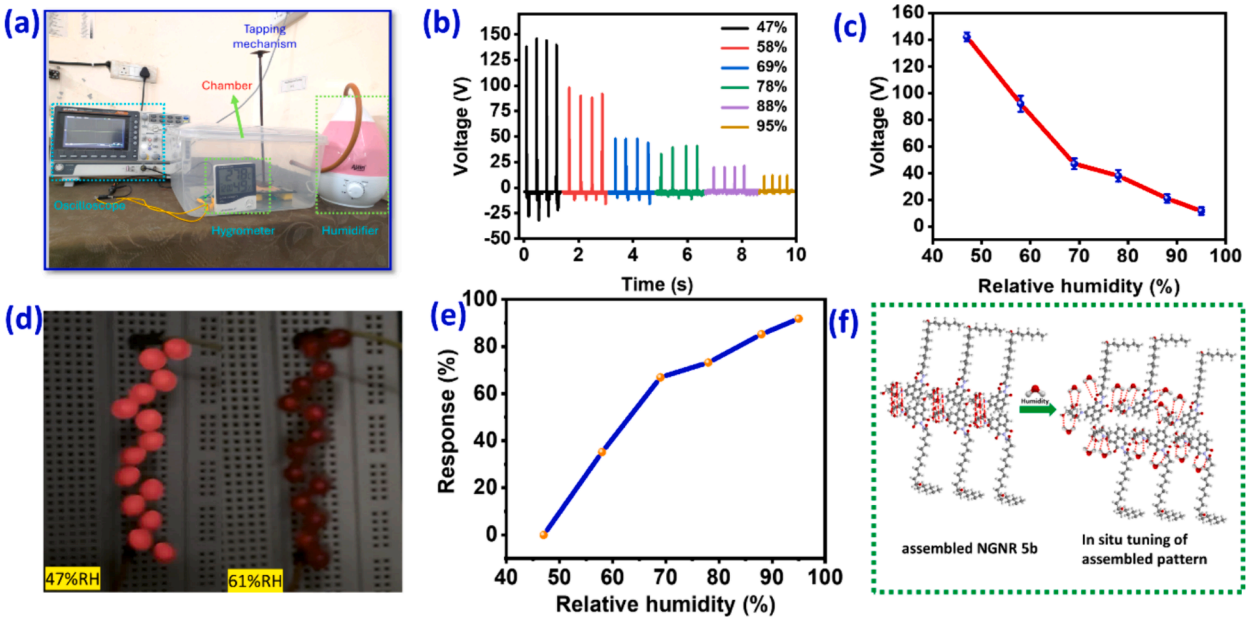

Fig. 5. (a) Photograph of the humidity sensing set up, (b)-(c) TENG output voltage under different humidity conditions with statistical analysis data, (d) Photograph of the LEDs powered by TENG under two different humidity levels, (e) Response plot of TENG with humidity variation, (f) proposed humidity sensing mechanism. Experiments are performed in triplicate under optimized conditions to check the reproducibility and repeatability.

analysis of TENG data. **Subbiah Nagarajan:** Conceptualization, Methodology, Investigation, Analysis, Software, Fund Acquisition, Writing – original draft, review & editing.

Declaration of competing interest

The authors declare the following financial interests/personal relationships which may be considered as potential competing interests: Subbiah Nagarajan reports financial support was provided by Science and Engineering Research Board. Subbiah Nagarajan has patent granted on SYNTHESIS OF AMPHIPHILIC N-GLYCOSYL NAPHTHALIMIDES AND FABRICATION OF FLEXIBLE SEMICONDUCTOR USING MOLECULAR SELF-ASSEMBLY bearing patent No. 524613. There is NO conflict of Interest to disclose If there are other authors, they declare that they have no known competing financial interests or personal relationships that could have appeared to influence the work reported in this paper.

Data availability

No data was used for the research described in the article.

Acknowledgments

We greatly acknowledge the financial support from the SERB (sanction order no: CRG/2023/002466) and DST FIST (SR/FST/CS-II/2018/65). The authors thank the National Institute of Technology Warangal for the infrastructure facilities. We also thank C Uma Maheswari, SASTRA University, and Vellaisamy Sridharan, Central University of Jammu, for data acquisition help.

Appendix A. Supplementary data

Supplementary data to this article can be found online at https://doi.org/10.1016/j.cej.2024.151800.

References

[1] S. Sicari, A. Rizzardi, A. Coen-Porisini, 5G In the internet of things era: An overview on security and privacy challenges, Comput. Netw. 179 (2020) 107345.
[2] H. Hui, Y. Ding, Q. Shi, F. Li, Y. Song, J. Yan, 5G network-based Internet of Things for demand response in smart grid: A survey on application potential, Appl. Energy 257 (2020) 113972.
[3] K.A. Cook-Chennault, N. Thambi, A.M. Sastry, Powering MEMS portable devices—a review of non-regenerative and regenerative power supply systems with special emphasis on piezoelectric energy harvesting systems, Smart Mater. Struct. 17 (2008) 43001.
[4] D. Zhang, Q. Liu, Biosensors and bioelectronics on smartphone for portable biochemical detection, Biosens. Bioelectron. 75 (2016) 273–284.
[5] X. Lu, P. Wang, D. Niyato, D.I. Kim, Z. Han, Wireless networks with RF energy harvesting: A contemporary survey, IEEE Commun. Surv. Tutorials 17 (2015) 757–789.
[6] J. Yick, B. Mukherjee, D. Ghosal, Wireless sensor network survey, Comput. Netw. 52 (2008) 2292–2330.
[7] Z.L. Wang, T. Jiang, L. Xu, Toward the blue energy dream by triboelectric nanogenerator networks, Nano Energy 39 (2017) 9–23.
[8] Y. Zi, H. Guo, Z. Wen, M.-H. Yeh, C. Hu, Z.L. Wang, Harvesting low-frequency (<5 Hz) irregular mechanical energy: a possible killer application of triboelectric nanogenerator, ACS Nano 10 (2016) 4797–4805.
[9] X. Peng, K. Dong, C. Ye, Y. Jiang, S. Zhai, R. Cheng, D. Liu, X. Gao, J. Wang, Z. L. Wang, A breathable, biodegradable, antibacterial, and self-powered electronic skin based on all-nanofiber triboelectric nanogenerators, Sci. Adv. 6 (2020) eaba9624.
[10] S. Mahalingam, A. Manap, K.S. Lau, D. Floresyona, R. Medali Rachman, S. Ayu Pradanawati, R. Rabeya, C.H. Chia, N. Afandi, A. Nugroho, Review of bioresource-based conductive composites for portable flexible electronic devices, Renew. Sustain. Energy Rev. 189 (2024).
[11] C. Zhang, Z.L. Wang, Triboelectric nanogenerators BT - micro electro mechanical systems, in: Q.-.-A. Huang (Ed.), Springer Singapore, Singapore, 2018, pp. 1335–1376.
[12] G. Zhu, B. Peng, J. Chen, Q. Jing, Z., Lin Wang, Triboelectric nanogenerators as a new energy technology: From fundamentals, devices, to applications, Nano Energy 14 (2014) 126–138.
[13] H. Zou, Y. Zhang, L. Guo, P. Wang, X. He, G. Dai, H. Zheng, C. Chen, A.C. Wang, C. Xu, Z.L. Wang, Quantifying the triboelectric series, Nat. Commun. 10 (2019) 1427.
[14] G. Khandelwal, A. Chandrasekhar, N.P. Maria Joseph Raj, S.-J. Kim, Metal-organic framework: A novel material for triboelectric nanogenerator-based self-powered sensors and systems, Adv. Energy Mater. 9 (2019) 1803581.
[15] S. Rathore, S. Sharma, B.P. Swain, R.K. Ghadai, A critical review on triboelectric nanogenerator, IOP Conf. Ser. Mater. Sci. Eng. 377 (2018) 12186.
[16] F.-R. Fan, Z.-Q. Tian, Z. Lin Wang, Flexible triboelectric generator, Nano Energy 1 (2012) 328–334, https://doi.org/10.1016/j.nanoen.2012.01.004.
[17] W. Yang, X. Cai, S. Guo, L. Wen, Z. Sun, R. Shang, X. Shi, J. Wang, H. Chen, Z. Li, A high performance triboelectric nanogenerator based on mxene/graphene oxide electrode for glucose detection, Materials (basel). 16 (2023) 841, https://doi.org/10.3390/ma16020841.
[18] H.A. Deveci, M. Mavioğlu Kaya, İ. Kaya, B. Bankoğlu Yola, N. Atar, M.L. Yola, Bisphenol A imprinted electrochemical sensor based on graphene quantum dots with boron functionalized g-C3N4 in food samples, Biosensors 13 (2023) 725, https://doi.org/10.3390/bios13070725.
[19] N. Çapar, B.B. Yola, İ. Polat, S. Bekerecioğlu, N. Atar, M.L. Yola, A zearalenone detection based on molecularly imprinted surface plasmon resonance sensor including sulfur-doped g-C3N4/Bi2S3 nanocomposite, Microchem. J. 193 (2023) 109141, https://doi.org/10.1016/j.microc.2023.109141.
[20] Ş.Y. Akıcı, B. Bankoğlu Yola, B. Karslıoğlu, İ. Polat, N. Atar, M.L. Yola, Fenpicoxamid-imprinted surface plasmon resonance (SPR) sensor based on sulfur-doped graphitic carbon nitride and its application to rice samples, Micromachines 15 (2024) 6, https://doi.org/10.3390/mi15010006.
[21] N.Ç. Rehman, N. Özdemir, H. Boyacıoğlu, M.L. Yola, A novel molecularly imprinted electrochemical sensor based on graphitic carbon nitride nanosheets decorated bovine serum albumin@MnO2 nanocomposite for zearalenone detection, J. Food Compos. Anal. 125 (2024) 105857, https://doi.org/10.1016/j.jfca.2023.105857.
[22] N. Özdemir, B. Karslıoğlu, B. Bankoğlu Yola, N. Atar, M.L. Yola, A novel molecularly imprinted quartz crystal microbalance sensor based on erbium molybdate incorporating sulfur-doped graphitic carbon nitride for dimethoate determination in apple juice samples, Foods 13 (2024) 810, https://doi.org/10.3390/foods13050810.
[23] B. Demir, B.B. Yola, S. Bekerecioğlu, İ. Polat, M.L. Yola, A nivalenol imprinted quartz crystal microbalance sensor based on sulphur-incorporating cobalt ferrite and its application to rice samples, Anal. Methods 16 (2024) 1215–1224, https://doi.org/10.1039/d4ay00008k.
[24] A. Nourizad, S. Golmohammadi, A. Aghanejad, M.R. Tohidkia, Recent trends in aptamer-based nanobiosensors for detection of vascular endothelial growth factors (VEGFs) biomarker: A review, Environ. Res. 236 (2023) 116726, https://doi.org/10.1016/j.envres.2023.116726.
[25] C. Karaman, B.B. Yola, O. Karaman, N. Atar, İ. Polat, M.L. Yola, Sensitive sandwich-type electrochemical SARS-CoV-2 nucleocapsid protein immunosensor, Microchim. Acta 188 (2021) 425, https://doi.org/10.1007/s00604-021-05092-6.
[26] M.L. Yola, Sensitive sandwich-type voltammetric immunosensor for breast cancer biomarker HER2 detection based on gold nanoparticles decorated Cu-MOF and Cu2ZnSnS4 NPs/Pt/g-C3N4 composite, Microchim. Acta 188 (2021), https://doi.org/10.1007/s00604-021-04735-y.
[27] M.L. Yola, N. Atar, Amperometric galectin-3 immunosensor-based gold nanoparticle-functionalized graphitic carbon nitride nanosheets and core-shell Ti-MOF@COFs composites, Nanoscale 12 (2020) 19824–19832, https://doi.org/10.1039/d0nr05614f.
[28] S. Kadirsoy, N. Atar, M.L. Yola, Molecularly imprinted QCM sensor based on delaminated MXene for chlorpyrifos detection and QCM sensor validation, New J. Chem. 44 (2020) 6524–6532, https://doi.org/10.1039/d0nj00951b.
[29] N. Özcan, H. Medetalibeyoglu, O. Akyıldırım, N. Atar, M.L. Yola, Electrochemical detection of amyloid-β protein by delaminated titanium carbide MXene/multi-walled carbon nanotubes composite with molecularly imprinted polymer, Mater. TodayCommun. 23 (2020) 101097, https://doi.org/10.1016/j.mtcomm.2020.101097.
[30] M. Yola, N. Atar, A. Review, Molecularly imprinted electrochemical sensors for determination of biomolecules/drug, Curr. Anal. Chem. 13 (2017) 13–17, https://doi.org/10.2174/1573411012666160601141018.
[31] A.K. Rachamalla, S. Potu, V.P. Rebaka, T. Banoo, Y. Kumar, C.U. Maheswari, V. Sridharan, R.K. Rajaboina, S. Nagarajan, Electronically robust self-assembled supramolecular gel as a potential material in triboelectric nanogenerators, Chem. - A Eur. J. 29 (2023).
[32] S.M. Nawaz, M. Chatterjee, S. Chakrabarti, N. Sepay, A. Mallik, Realization of a highly-performing triboelectric nanogenerator utilizing molecular self-assembly, Nano Energy 117 (2023) 108924.
[33] P.C. Calder, Functional roles of fatty acids and their effects on human health, J. Parenter. Enter. Nutr. 39 (2015) 18S–32S.
[34] D.A.J. Stone, Dietary carbohydrate utilization by fish, Rev. Fish. Sci. 11 (2003) 337–369.
[35] J.D. Mul, K.I. Stanford, M.F. Hirshman, L.J. Goodyear, Exercise and regulation of carbohydrate metabolism, Prog. Mol. Biol. Transl. Sci. 135 (2015) 17–37.
[36] R. Tyagi, K. Singh, N. Srivastava, R. Sagar, Recent advances in carbohydrate-based gelators, Mater. Adv. 4 (2023) 3929–3950.
[37] B.M. Turner, Cellular memory and the histone code, Cell 111 (2002) 285–291.
[38] K. Ohtsubo, J.D. Marth, Glycosylation in cellular mechanisms of health and disease, Cell 126 (2006) 855–867.
[39] A. Kobata, Structures and functions of the sugar chains of glycoproteins, Eur. J. Biochem. 209 (1992) 483–501.
[40] D.C. Fork, S.K. Herbert, Electron transport and photophosphorylation by Photosystem I in vivo in plants and cyanobacteria, Photosynth. Res. 36 (1993) 149–168.

[41] J.E. Holesh, S. Aslam, A. Martin, Physiology, carbohydrates. Treasure Island (FL), 2024.
[42] A. Sidar, E.D. Albuquerque, G.P. Voshol, A.F.J. Ram, E. Vijgenboom, P.J. Punt, Carbohydrate binding modules: diversity of domain architecture in amylases and cellulases from filamentous microorganisms, Front. Bioeng. Biotechnol. 8 (2020) 1–15.
[43] A. Kirui, W. Zhao, F. Deligey, H. Yang, X. Kang, F. Mentink-Vigier, T. Wang, Carbohydrate-aromatic interface and molecular architecture of lignocellulose, Nat. Commun. 13 (2022) 538.
[44] S. Pérez, I. Tvaroška, Carbohydrate-protein interactions: molecular modeling insights, Adv. Carbohydr. Chem. Biochem. 71 (2014) 9–136.
[45] E. Jéquier, Carbohydrates as a source of energy, Am. J. Clin. Nutr. 59 (1994) 682S–S685.
[46] H.F. Oldenkamp, J.E. Vela Ramirez, N.A. Peppas, Re-evaluating the importance of carbohydrates as regenerative biomaterials, Regen. Biomater. 6 (2019) 1–12.
[47] L. Li, G. Chen, Precise assembly of proteins and carbohydrates for next-generation biomaterials, J. Am. Chem. Soc. 144 (2022) 16232–16251.
[48] M.D. Tomczyk, K.Z. Walczak, l,8-Naphthalimide based DNA intercalators and anticancer agents. A systematic review from 2007 to 2017, Eur. J. Med. Chem. 159 (2018) 393–422.
[49] A. Zhang, Y. Zhang, Z. Xu, Y. Li, X. Yu, L. Geng, Naphthalimide-based fluorescent gelator for construction of both organogels and stimuli-responsive metallogels, RSC Adv. 7 (2017) 25673–25677.
[50] S. Kagatikar, D. Sunil, A systematic review on 1,8-naphthalimide derivatives as emissive materials in organic light-emitting diodes, J. Mater. Sci. 57 (2022) 105–139.
[51] R. Greiner, T. Schlücker, D. Zgela, H. Langhals, Fluorescent aryl naphthalene dicarboximides with large Stokes shifts and strong solvatochromism controlled by dynamics and molecular geometry, J. Mater. Chem. C 4 (2016) 11244–11252.
[52] M. Poddar, G. Sivakumar, R. Misra, Donor-Acceptor substituted 1,8-naphthalimides: Design, synthesis, and structure-property relationship, J. Mater. Chem. C 7 (2019) 14798–14815.
[53] P. Gopikrishna, N. Meher, P.K. Iyer, Functional 1,8-naphthalimide AIE/AIEEgens: recent advances and prospects, ACS Appl. Mater. Interfaces 10 (2018) 12081–12111.
[54] W. Johnson, Final report on the safety assessment of ricinus communis (castor) seed oil, hydrogenated castor oil, glyceryl ricinoleate, glyceryl ricinoleate SE, ricinoleic acid, potassium ricinoleate, sodium ricinoleate, zinc ricinoleate, cetyl ricinoleate, ethyl ric, Internat. J. Toxicol. 26 (2007) 31–77.
[55] M. Lv, H. Xu, Overview of naphthalimide analogs as anticancer agents, Curr. Med. Chem. 16 (2009) 4797–4813.
[56] A.L. Berhanu, I. Mohiuddin, A.K. Malik, J.S. Aulakh, V. Kumar, K.-H. Kim, A review of the applications of Schiff bases as optical chemical sensors, TrAC - Trends Anal. Chem. 116 (2019) 74–91.
[57] Y. Wang, X. Zhao, Y. Liu, W. Zhou, The effect of metal surface nanomorphology on the output performance of a TENG, Beilstein J. Nanotechnol. 13 (2022) 298–312.
[58] Y. Zou, J. Xu, K. Chen, J. Chen, Advances in nanostructures for high-performance triboelectric nanogenerators, Adv. Mater. Technol. 6 (2021) 2000916.
[59] M. Ibrahim, J. Jiang, Z. Wen, X. Sun, Surface engineering for enhanced triboelectric nanogenerator, Nanoenergy Adv. 1 (2021) 58–80.
[60] Y. Zheng, L. Cheng, M. Yuan, Z. Wang, L. Zhang, Y. Qin, T. Jing, An electrospun nanowire-based triboelectric nanogenerator and its application in a fully self-powered UV detector, Nanoscale 6 (2014) 7842–7846.
[61] T. Bhatta, S. Sharma, K. Shrestha, Y. Shin, S. Seonu, S. Lee, D. Kim, M. Sharifuzzaman, S.M.S. Rana, J.Y. Park, Siloxene/PVDF composite nanofibrous membrane for high-performance triboelectric nanogenerator and self-powered static and dynamic pressure sensing applications, Adv. Funct. Mater. 32 (2022) 2202145.
[62] X. Pu, L. Li, H. Song, C. Du, Z. Zhao, C. Jiang, G. Cao, W. Hu, Z.L. Wang, A self-charging power unit by integration of a textile triboelectric nanogenerator and a flexible lithium-ion battery for wearable electronics, Adv. Mater. 27 (2015) 2472–2478.
[63] S. Potu, N. Madathil, S. Mishra, A. Bora, Y. Sivalingam, A. Babu, M. Velpula, L. Bochu, B. Ketharachapalli, A. Kulandaivel, R.K. Rajaboina, U.K. Khanapuram, H. Divi, P. Kodali, B. Murali, R. Ketavath, Surface-engineered high-performance triboelectric nanogenerator for self-powered health monitoring and electronics, ACS Appl. Eng. Mater. 1 (2023) 2663–2675.
[64] M. Navaneeth, S. Potu, A. Babu, B. Lakshakoti, R.K. Rajaboina, U. Kumar, K. H. Divi, P. Kodali, K. Balaji, Transforming medical plastic waste into high-performance triboelectric nanogenerators for sustainable energy, health monitoring, and sensing applications, ACS Sustain. Chem. Eng. 11 (2023) 12145–12154.
[65] M. Rakshita, N. Madathil, A.A. Sharma, P.P. Pradhan, D.P. Kasireddi, U. K. Khanapuram, R.K. Rajaboina, H. Divi, Phosphor-based triboelectric nanogenerators for mechanical energy harvesting and self-powered systems, ACS Appl. Electron. Mater. (2024).
[66] P. Supraja, R.R. Kumar, S. Mishra, D. Haranath, P.R. Sankar, K. Prakash, N. Jayarambabu, T.V. Rao, K.U. Kumar, A simple and low-cost triboelectric nanogenerator based on two dimensional ZnO nanosheets and its application in portable electronics, Sens. Actuators, A 335 (2022) 113368.
[67] S. Panda, H. Jeong, S. Hajra, P.M. Rajaitha, S. Hong, H.J. Kim, Biocompatible polydopamine based triboelectric nanogenerator for humidity sensing, Sensors Actuators B Chem. 394 (2023) 134384.
[68] D. Zhang, Y. Yang, Z. Xu, D. Wang, C. Du, An eco-friendly gelatin based triboelectric nanogenerator for a self-powered PANI nanorod/NiCo2O4 nanosphere ammonia gas sensor, J. Mater. Chem. A 10 (2022) 10935–10949.
[69] C. Huang, G. Chen, A. Nashalian, J. Chen, Advances in self-powered chemical sensing via a triboelectric nanogenerator, Nanoscale 13 (2021) 2065–2081.
[70] Z.L. Wang, Triboelectric nanogenerators as new energy technology for self-powered systems and as active mechanical and chemical sensors, ACS Nano 7 (2013) 9533–9557.
[71] S. Sardana, Z. Singh, A.K. Sharma, N. Kaur, P.K. Pati, A. Mahajan, Self-powered biocompatible humidity sensor based on an electrospun anisotropic triboelectric nanogenerator for non-invasive diagnostic applications, Sensors Actuators B Chem. 371 (2022) 132507.
[72] F. Ejehi, R. Mohammadpour, E. Asadian, S. Fardindoost, P. Sasanpour, Enhancement of self-powered humidity sensing of graphene oxide-based triboelectric nanogenerators by addition of graphene oxide nanoribbons, Mikrochim. Acta 188 (2021) 251.
[73] Z. Duan, Y. Jiang, H. Tai, Recent advances in humidity sensors for human body related humidity detection, J. Mater. Chem. C 9 (2021) 14963–14980.
[74] D. Jung, J. Kim, G.S. Lee, Enhanced humidity-sensing response of metal oxide coated carbon nanotube, Sens. Actuators, A 223 (2015) 11–17.
[75] V. Mohan, V.K. Mariappan, P. Pazhamalai, K. Krishnamoorthy, S.J. Kim, Unravelling the impact of carbon allotropes in flexible polydimethylsiloxane film towards self-powered triboelectric humidity sensor, Carbon N. Y. 205 (2023) 328–335.
[76] L. Zhang, H. Li, Y. Xie, J. Guo, Z. Zhu, Triboelectric nanogenerator based on teflon/vitamin B1 powder for self-powered humidity sensing, Beilstein J. Nanotechnol. 11 (2020) 1394–1401.
[77] V. Nguyen, R. Yang, Effect of humidity and pressure on the triboelectric nanogenerator, Nano Energy 2 (2013) 604–608.